Design and Simulation of Fully Printable Conformal Antennas with BST/Polymer Composite Based Phase Shifters

Mahdi Haghzadeh[1], Hamzeh Jaradat[2], Craig Armiento[1], and Alkim Akyurtlu[1, *]

Abstract—A fully printable and conformal antenna array on a flexible substrate with a new Left-Handed Transmission Line (LHTL) phase shifter based on a tunable Barium Strontium Titanate (BST)/polymer composite is proposed and computationally studied for radiation pattern correction and beam steering applications. First, the subject 1×4 rectangular patch antenna array is configured as a curved conformal antenna, with both convex and concave bending profiles, and the effects of bending on the performance are analyzed. The maximum gain of the simulated array is reduced from the flat case level by 34.4% and 34.5% for convex and concave bending, respectively. A phase compensation technique utilizing the LHTL phase shifters with a coplanar design is used to improve the degraded radiation patterns of the conformal antennas. Simulations indicate that the gain of the bent antenna array can be improved by 63.8% and 68% for convex and concave bending, respectively. For the beam steering application, the proposed phase shifters with a microstrip design are used to steer the radiation beam of the antenna array, in planar configuration, to both negative and positive scan angles, thus realizing a phased array antenna.

1. INTRODUCTION

Printed flexible electronics is a promising approach for developing electronic and electromagnetic subsystems with different form factors. The potential advantages of printed electronics include ultra-low cost, rapid prototyping, low temperature processing, and roll-to-roll manufacturing on flexible plastic substrates. The ability to print electronic materials on flexible thin substrates has been exploited for radio frequency (RF) communication components such as filters [1], transistors [2, 3], switches [4] and antennas [5–7]. Among various antenna types, microstrip antennas are particularly desirable for numerous wireless applications due to their simplicity, low cost, low profile, conformability to curved surfaces, and versatility in design [8]. The flexibility of the substrate adds a degree of freedom in the antenna design since the substrate can be incorporated on curved surfaces as a conformal antenna. Examples of conformal antennas vary from avionics antennas, where bending the antenna to conform to the curved surface of an aircraft reduces the aerodynamic drag [9], to wearable antennas, where conformal antennas provide the freedom to design body-worn, light, and less visually intrusive antennas [10]. Although conformability can be advantageous in many aspects, bending the array can result in performance degradation (e.g., gain) compared with a conventional planar array [11]. Many attempts have been made to study and address the deteriorative effects of bending on radiation pattern of conformal antennas [12–14]. In a more recent work, an autonomous self-adapting capability is developed for a flexible microstrip antenna array by utilizing locally based sensors and a feedback analog circuit to detect and recover the pattern of the conformal antenna array for different deformations [15]. In previously reported studies including the latter work, compensation is commonly achieved by locating

[1] Department of Electrical and Computer Engineering, University of Massachusetts Lowell, Lowell, MA 01854, USA. [2] Department of Electrical and Computer Engineering, Yarmouk University, Irbid, Jordan.

a commercially available tunable phase shifter at the feed line of the array elements to adjust the phase of the spatially displaced elements, thus recovering the distorted radiation pattern. However, the incorporation of such phase shifters increases the total cost of the system due to the increased complexity, additional fabrication steps, and greater number of elements [16]. Moreover, fully printed conformal antennas demand unique fabrication characteristics for phase shifters such as mechanical flexibility and printability. In order to fully print a conformal planar antenna array with the capability to recover the degraded radiation pattern of a bent antenna, the key milestone is to develop a printable phase shifter design.

Phase shifters are key components in RF systems. In particular, in Phased Array Antenna (PAA) designs, it is necessary to control beam steering electronically using phase shifters at antenna feed lines. One approach to implement phase shifting is to switch between delay lines of different lengths. Several approaches have been pursued to design switching mechanisms for phase shifters, including Monolithic Microwave Integrated Circuits (MMICs) and RF Micro-electromechanical Systems (MEMS) approaches. The drawback of such technologies is that they often require an expensive packaging and chip integration. Recently, a flexible printed conformal phased array antenna was introduced by using active membrane phased-array for radar applications [17]. Another recent advance in the development of lightweight flexible PAAs is based on a Liquid Crystal Polymer (LCP) substrate [18]. Carbon Nano-tubes (CNTs) have also been used to print Thin-film Transistors (CNT-TFTs) [19], which can be used as a switch between the delay-line feeding network to control a 2-bit two-element printed PAA [20]. Flexible printed circuits [21], or stamped antennas, have also been reported, using silver nano-inks for printing the feed lines and power dividers. The same method is used in [22, 23] with ink-jet printed 2-bit, 1×4 PAA system on a flexible Kapton polyimide substrate utilizing CNT-TFTs as switching elements in the phase-shifting network. Beam steering is achieved by controlling the ON/OFF states of the transistors. The drawback of the switched line method is that it usually provides a limited degree of tunability with digitized states. On the other hand, the complexity and cost of a phased array system could be reduced by a passive antenna array approach, while its size could be reduced by a tunable compact phase shifter.

One promising approach to create a compact tunable phase shifter is to use ferroelectric materials such as Barium Strontium Titanate (BST), whose relative permittivity can be tuned by applying an electrostatic field. BST-based phase shifters have advantages such as compactness, low power consumption, adequate tunability, tolerable dielectric loss and high tuning speed [24]. However, thick or thin films of BST suffer from rigidity and high temperature processing ($> 850°C$), which make their use impractical in printed electronics on flexible substrates. This paper proposes to eliminate these shortcomings by using a 0–3 type BST/polymer composite made by suspending micro- or nano-sized BST particles in a polymer matrix. Such a solution is a compromise between the processing flexibility of a polymer and the desired ferroelectric properties of BST. The fabrication and material properties of many BST/polymer composites have been reported using various polymers such as silicon-rubber [25], epoxy resin [26], polymethylmethacrylate (PMMA) [27], polyphenylene sulfide (PPS) [28], and cyclic olefin copolymer (COC) [29]. In a previous work, we reported our progress in developing tunable BST/polymer composites to fabricate printed varactors for flexible, tunable Frequency Selective Surfaces (FSSs) [30]. In another recent work, we printed BST/COC dielectrics using an ink, and developed a novel RF measurement technique to characterize their complex dielectric properties with a dielectric constant of $\varepsilon_r = 35$ and a loss tangent of $\tan \delta = 0.01$ at $f = 10\,\text{GHz}$ [31]. In this work, we integrate the concept of tunable BST/polymer composite with a previously reported BST-based phase shifter design that is comprised of a Left Handed Transmission Line (LHTL) made up of a series of Interdigitated Capacitors (IDCs) with shunt inductors realized by short stubs [16]. The novelty of our design is due to the use of ferroelectric BST/polymer material in multiphase composite form that can be additively filled in between the IDC fingers, as opposed to the conventional BST-based phase shifters, where IDC fingers are fabricated on a thick or thin film of BST. In our approach, the BST material is placed between the IDC fingers where the electric field is strongest, thus leading to higher capacitance-per-area and possibly less required tuning voltage, as we have analyzed analytically and computationally in a previous work [32].

Here, we computationally study the realization of conformal antenna arrays by integrating the proposed BST/polymer composite based LHTL phase shifters in antenna arrays in order to: 1)

compensate the gain reduction of bent flexible antenna arrays, and 2) realize beam steering for planar phased arrays. This new phase shifter design is compatible with additive manufacturing processes and can reduce fabrication steps, overall size and complexity, and hence the total cost of the system. This paper is organized as follows. In Section 2, BST/polymer-based LHTL phase shifters are presented with both coplanar and microstrip designs, as well as the phase tuning mechanism. In Section 3, the design of a 1×4 rectangular patch antenna array used in this study is described. In Section 4, two bending configurations are studied for the patch antenna array with an emphasis on the effect of bending on antenna gain. The phase shift caused by bending the antennas is calculated, and a phase compensation approach utilizing BST/polymer-based LHTL phase shifters is used to compensate the gain. Section 5 demonstrates how BST/polymer-based LHTL phase shifters with radial stubs can be utilized to electrically beam steer the main beam of the array. A summary is provided in Section 6.

2. BST/POLYMER BASED LHTL PHASE SHIFTERS

Left Handed Transmission Lines (LHTLs), also called artificial or metamaterial lines, consist of a unit cell including a series capacitance, C, and a shunt inductance, L, contrary to that of Right Handed Transmission Lines (RHTLs), which include a series inductance, L, and a shunt capacitance, C. This leads to an inverse propagation constant, as shown below [33]:

$$\gamma_{\text{LHTL}} = \frac{1}{\gamma_{\text{RHTL}}} = \frac{1}{j\omega\sqrt{LC}} \tag{1}$$

The detailed theory, circuit analysis, and application of Composite Right/Left Handed (CRLH) Transmission Lines (TLs) are reported in [33]. The main advantages of LHTLs (a subset of CRLH TLs) include their compactness (due to a larger phase constant) and higher sensitivity to capacitance tunability within a particular frequency range, compared to their RHTL counterparts [16, 34–36]. Moreover, it has been shown that the combination of LHTL with the BST leads to an almost constant magnitude over the tuning states [16]. A tunable propagation constant is achieved by employing a tunable capacitor in the unit cell. The most common design is the conventional BST-based IDC, where interdigitated fingers are electroplated on a thick or thin film of BST in ceramic form. Fabrication of such films is impractical on flexible substrates since they require very high temperature ($> 850°$C) sintering processes [24]. As an alternative compatible with additive manufacturing techniques, a multiphase BST/polymer composite made by suspending nano/micro-size particles of BST in a polymer matrix can be utilized to obtain tunability [31]. The multiphase BST/polymer material can be directly deposited and filled in the gap between the fingers of IDCs in the LHTL. When used in BST/polymer form, no sintering is required as the composite material benefits from processing flexibilities of the polymer matrix. The dielectric constant of unsintered BST/polymer composites is typically one order of magnitude less than that of thick film BST. However, by printing the BST/polymer material between the IDC fingers, a metal-insulator-metal capacitor is realized that, in fact, is tilted by 90°. Therefore the BST/polymer material is under a stronger electric field of a vertical parallel-plate capacitor and its dielectric constant can be lower, compared to the a BST film that is under the parasitic electric field of an in-plane capacitance [32]. Changing the bias voltage applied on the plates will tune the dielectric constant, ε_r, of BST/polymer material, thus tuning the capacitance values and consequently the propagation constant.

2.1. LHTL Coplanar Design with Vias

In order to investigate the abovementioned approach, a Coplanar Waveguide (CPW) LHTL phase shifter made of 13 series IDCs and 12 shorted shunt stubs is studied here. The layout is shown in Fig. 1(a). Each IDC has six fingers with a width of 15 μm and a length of 85 μm, and a 15 μm gap between the fingers. The shorted stubs are 1200 μm long and 20 μm wide. The metallic features of the structure that are assumed to be perfect electric conductors (PECs) and have a thickness of 10.5 μm. In practice, the conductive features could be printed using printing technologies such as inkjet or Aerosol jet printing with conductive inks such as nano-silver inks. The substrate is assumed to be a Kapton sheet with a thickness of 0.254 mm. The top ground plane is connected to the bottom ground plane using cylindrical
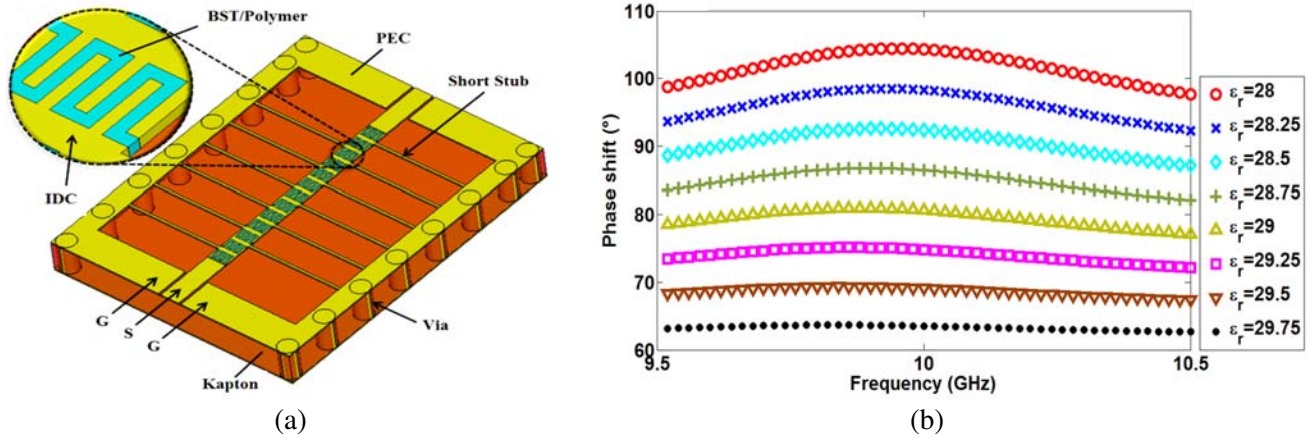
Figure 1. BST/polymer composite based CPW LHTL phase shifter: (a) schematic of the design, (b) simulated phase shifts in degrees for different values of dielectric constant.
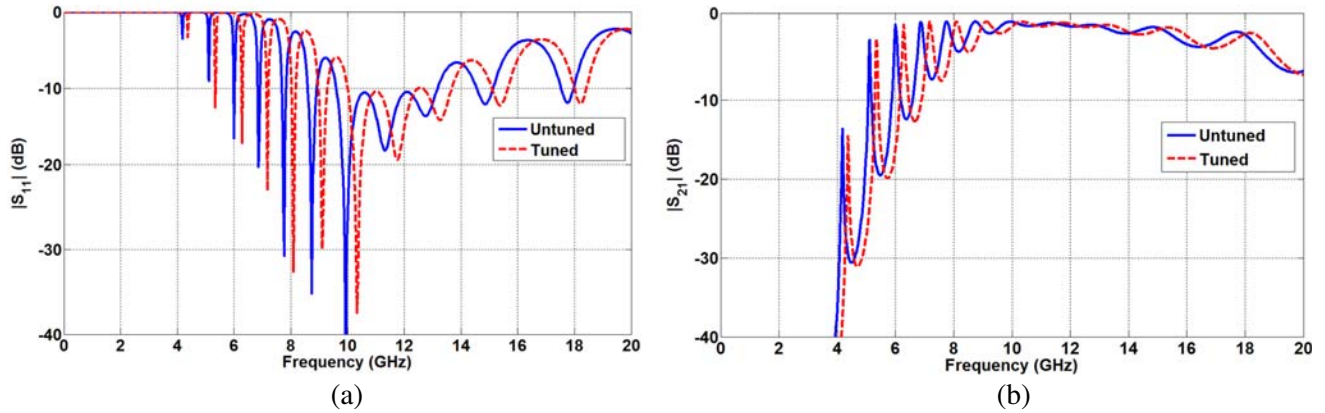
Figure 2. Simulated results of BST/polymer composite based CPW LHTL phase shifter: (a) $|S_{11}|$ in dB, and (b) simulated $|S_{21}|$ in dB.

vias. The spacing between the IDC fingers is filled with BST/polymer material. In order to simulate the dielectric tunability behavior of this material, its dielectric constant, ε_r, is parameter swept from 30 to 28, corresponding to a maximum tunability of 6.7%. In practice, the permittivity is tuned by applying a voltage across the material using a bias network. By tuning the permittivity of BST/polymer material, the capacitance values of series IDCs will change, thus tuning the phase of the transmitted RF signal. The phase difference curves as a function of frequency for various values of ε_r are shown in Fig. 1(b) at $f = 10$ GHz. All curves are calculated with respect to the phase reference at $\varepsilon_r = 30$. Simulated return and transmission losses at tuned ($\varepsilon_r = 28$) and untuned ($\varepsilon_r = 30$) states for the phase shifter are shown in Fig. 2(a) and Fig. 2(b), respectively. The phase shifter operates in a wide frequency range from 10 to 12.5 GHz with a maximum insertion loss of 2 dB and a maximum reflection loss of 10 dB.

2.2. LHTL Microstrip Design with Radial Stubs

The phase shifter discussed earlier requires an impedance-matched transition between the microstrip lines of an antenna array to the coplanar LHTL. It also requires fabricating grounding vias between the top conductors and the bottom ground plane. These increase the complexity of the design and produce fabrication challenges especially for printed electronics processes on flexible substrates. One solution to this problem is to replace the coplanar LHTL with a microstrip LHTL. The grounding vias

are replaced with radial open stubs that offer virtual grounding at the resonance frequency [16, 37]. The top view of the microstrip LHTL with radial stubs is shown in Fig. 3(a). The microstrip radial stubs have a radius of 3.29 mm and an angle of 76°, obtained based on optimization simulations. The material between the IDC fingers is again assumed to be the ferroelectric BST/polymer dielectric. The phase shift curves for this LHTL are plotted in Fig. 3(b) for various ε_r values. Simulations showed that this phase shifter had insertion and reflection losses similar to the CPW version of it in the desired frequency range. It is worth noting that the line impedance of LHTL slightly changes in a tuned state since the capacitance of the IDCs decreases as ε_r of the BST/polymer dielectric decreases. This will result in a reduced transmission, and hence a lower overall gain. However, the quality factor of BST material tends to increase in the tuned state [16], which will compensate for the degrading effects of line impedance mismatching.
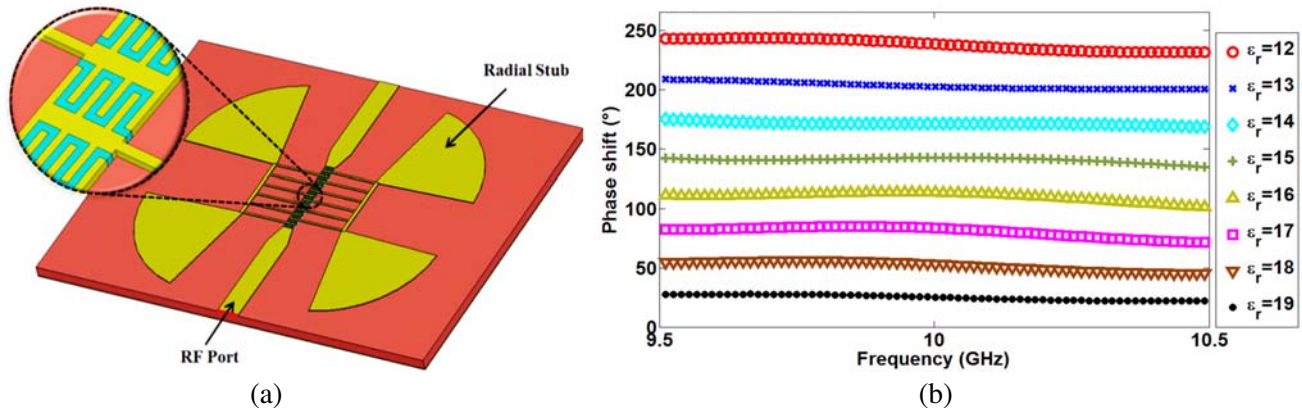
Figure 3. BST/polymer composite based LHTL phase shifter with radial stubs: (a) schematic of the design, (b) simulated phase shifts in degrees for various values of the dielectric constant.
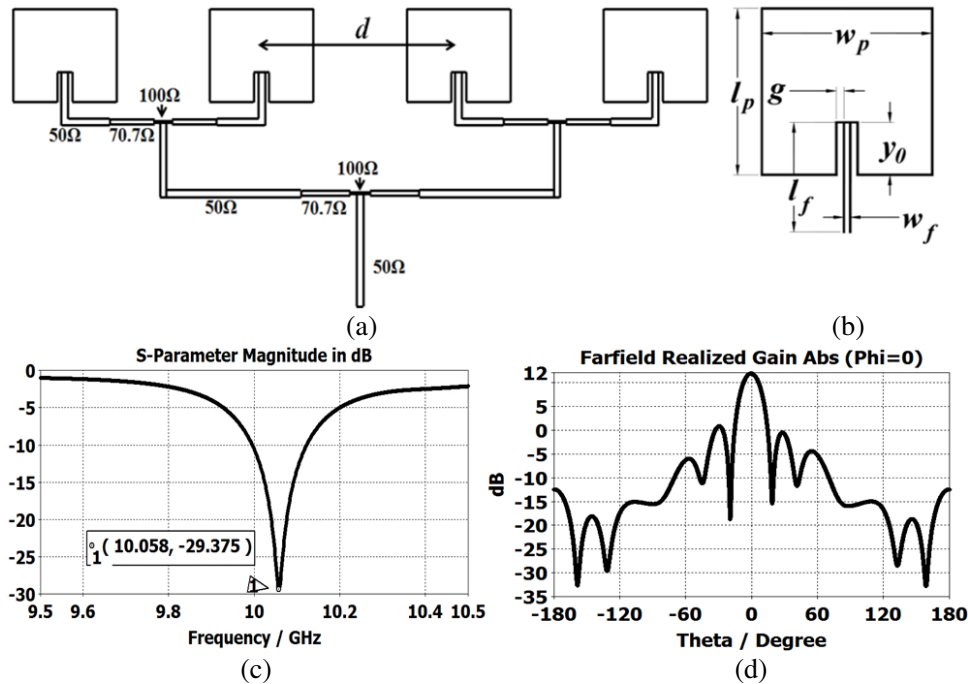
Figure 4. Rectangular patch antenna: (a) top view of a 1×4 array, (b) top view of a single patch, (c) $|S_{11}|$ in dB, (d) realized farfield gain in dB at resonance.

3. PATCH ANTENNA DESIGN

The antenna subject to this study is a rectangular 1×4 patch antenna array depicted in Fig. 4(a). Fig. 4(b) shows the top view of a single patch and the design parameters. The dimensions of each patch and the spacing between them are listed in Table 1 in millimeters. All dimensions are designed to give a resonance at $f = 10\,\text{GHz}$, which are all obtained by following the microstrip antenna design procedure presented in [8]. The center to center distance between the adjacent patches is $d = 25.16\,\text{mm}$. All feed lines are designed to match a $50\,\Omega$ line input. The design of the power splitter solution follows our previously reported work [38]. The width of each line of the power splitter is as follows; $w_{50\,\Omega} = 0.62\,\text{mm}$, $w_{70.7\,\Omega} = 0.42\,\text{mm}$, and $w_{100\,\Omega} = 0.2\,\text{mm}$. CST Microwave Studio was used to simulate the performance of the array. The simulated reflection coefficient, $|S_{11}|$, is shown in Fig. 4(c), where the resonant frequency occurs at $f = 10.058\,\text{GHz}$. The simulated realized gain versus scan angle, θ, at the resonance frequency is plotted in Fig. 4(d). The maximum main lobe gain is around $11.9\,\text{dB}$ and the beam width is approximately $16.9°$.

Table 1. Dimensions of the patch antenna array in millimeters (see Fig. 4(b) for the defined parameters).

w_P	l_P	y_0	w_f	l_f	g	h	d
7.92	7.92	2.8	0.62	8.39	0.45	0.3048	25.16

4. CONFORMAL ANTENNA ARRAY

4.1. Bending Effects on Antenna Array Performance

Deformation of an antenna array from a planar geometry to a non-planar geometry results in the distortion of the radiation pattern and consequently in the degradation in antenna performance, such as lower maximum gain and higher side lobe levels [15]. Here, we study two different bending profiles and the bending effects on the realized radiation pattern, following our previous work [38]. The convex (concave) geometry is realized by placing the patch antenna over the outer (inner) surface of a cylinder of radius, R, so that the inner (outer) surface of this cylinder is the ground plane. The radius is defined in terms of the operating wavelength, λ. The smaller radius corresponds to more bending. The radius
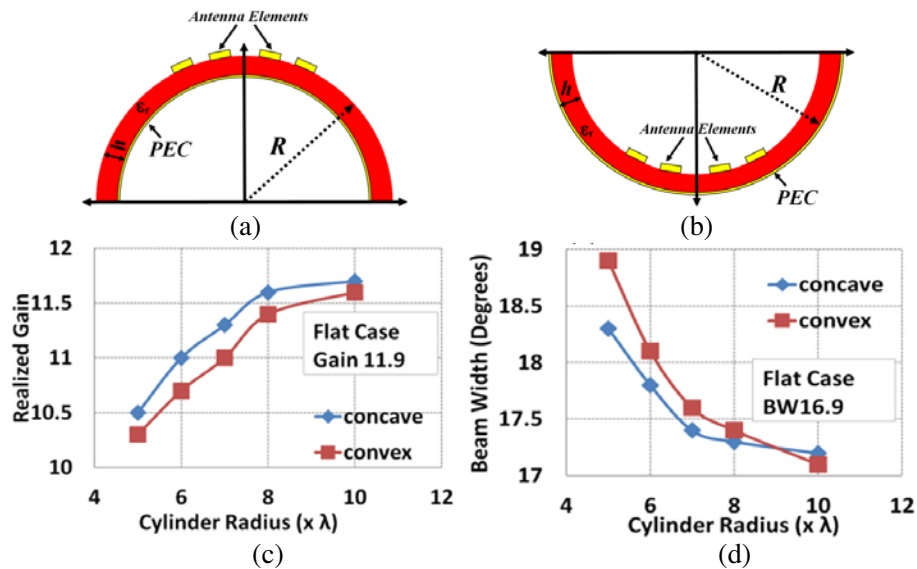
Figure 5. Schematic of the antenna array with (a) convex bending and (b) concave bending, and the bending effects for various concave and convex geometries (c) on the simulated maximum gain in dB and (d) on the beam width in degrees.

of the cylinder was decreased and each time the gain and beam width were recorded for both bending cases shown in Fig. 5(a) and Fig. 5(b). The plots of the maximum realized gain for both convex and concave bending as a function of the bending radius are plotted in Fig. 5(c).

As can be seen, the realized gain decreases significantly as the bending is increased by decreasing the bending radius. For instance, the gain drops from 11.6 dB to 10.3 dB when the radius changes from 10λ to 5λ for the convex case. The plots of the main lobe beam width for both convex and concave bending as a function of bending radius are plotted in Fig. 5(d). A broadening in the main lobe is observed as bending increases.

4.2. Phase Compensation

The bending of the surface alters the distances between the antenna elements [8, 15]. Consequently, the elements no longer lie on the same plane and significant vertical displacement appears. The result is a distorted radiation pattern and degraded overall performance. In order to restore the performance, the phase of appropriate array elements has to be modified. This could be done by incorporating phase shifters with the feed line of the elements. With this method, the phase of the surface current can be adjusted electrically to cancel out the spatial phase shift introduced by the bending. The amount of phase shift required for such compensations can be calculated based on the geometry of the conformal array [39]. Fig. 6 shows the geometry of a convex array in which the elements, labelled P1 to P4, are spatially displaced from their original flat positions. A new reference plane is realized at the level of inner elements (P2 and P3), and the outer elements (P1 and P4) are vertically displaced from this reference plane by an amount of Δz. When all the elements are excited with in-phase signals, the fields from outer elements will be delayed in phase at the reference plane by an amount of:

$$
\begin{aligned}
\Delta\phi = k\Delta z = kR\left|\sin(\phi_1) - \sin(\phi_2)\right| &= kR\left|\sin\left(\frac{\pi}{2} + \frac{3}{2}(\phi_1 - \phi_2)\right) - \sin\left(\frac{\pi}{2} + \frac{1}{2}(\phi_1 - \phi_2)\right)\right| \\
&= kR\left|\cos\left(\frac{3}{2}(\phi_1 - \phi_2)\right) - \cos\left(\frac{1}{2}(\phi_1 - \phi_2)\right)\right| = 2kR\left|\sin(\phi_1 - \phi_2)\sin\left(\frac{1}{2}(\phi_1 - \phi_2)\right)\right| \\
&= 2kR\left|\sin\left(\frac{d}{R}\right)\sin\left(\frac{d}{2R}\right)\right|
\end{aligned}
\tag{2}
$$

where k is the wave number of free space, d is the inter-element spacing, and R is the curvature radius. In other words, the Equation (2) calculates the phase shift required for the phase compensation method, i.e., $\Delta\phi$, based on the key geometry elements of the conformal antenna; namely, the curvature radius, R, and the inter-element spacing, d.

For an inter-element spacing of $d = 25.16$ mm and a bending radius of $R = 5\lambda$ for the model studied here, a required phase shift of $\Delta\phi = 89°$ is calculated using (2). In the convex case, the outer elements need to be advanced with this amount of phase in order to compensate for the deteriorated gain. Although this analysis is performed for the convex geometry, similar calculations could be performed for the concave bending as well, and similar phase shift is expected. However, in this case the inner elements (P2 and P3) need to be advanced in phase with this amount since these two elements are vertically displaced from the new reference plane by the amount of Δz.
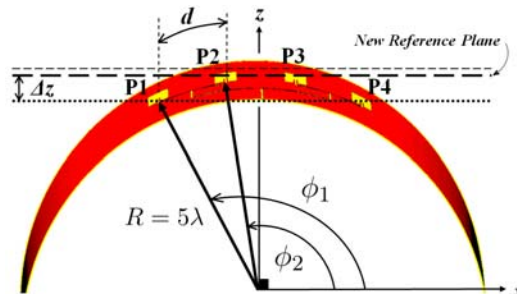
Figure 6. Convex bending geometry to calculate the required phase shift for gain compensation.

4.3. Pattern Correction in Conformal Antennas

We have calculated the required phase shift for phase compensation, $\Delta\phi$, using (2), and identified the appropriate elements to be advanced in phase by this amount of phase. In order to alleviate the deteriorating effects of bending on the performance of the conformal antenna array, the coplanar LHTL discussed in Section 2 can be used as a phase shifter and incorporated with the 1×4 array at the feed line of each element. This is shown in Fig. 7(a) for the convex bending and in Fig. 7(b) for the concave bending. The antenna is bent with a radius of $R = 5\lambda$. The phase shifters are labeled
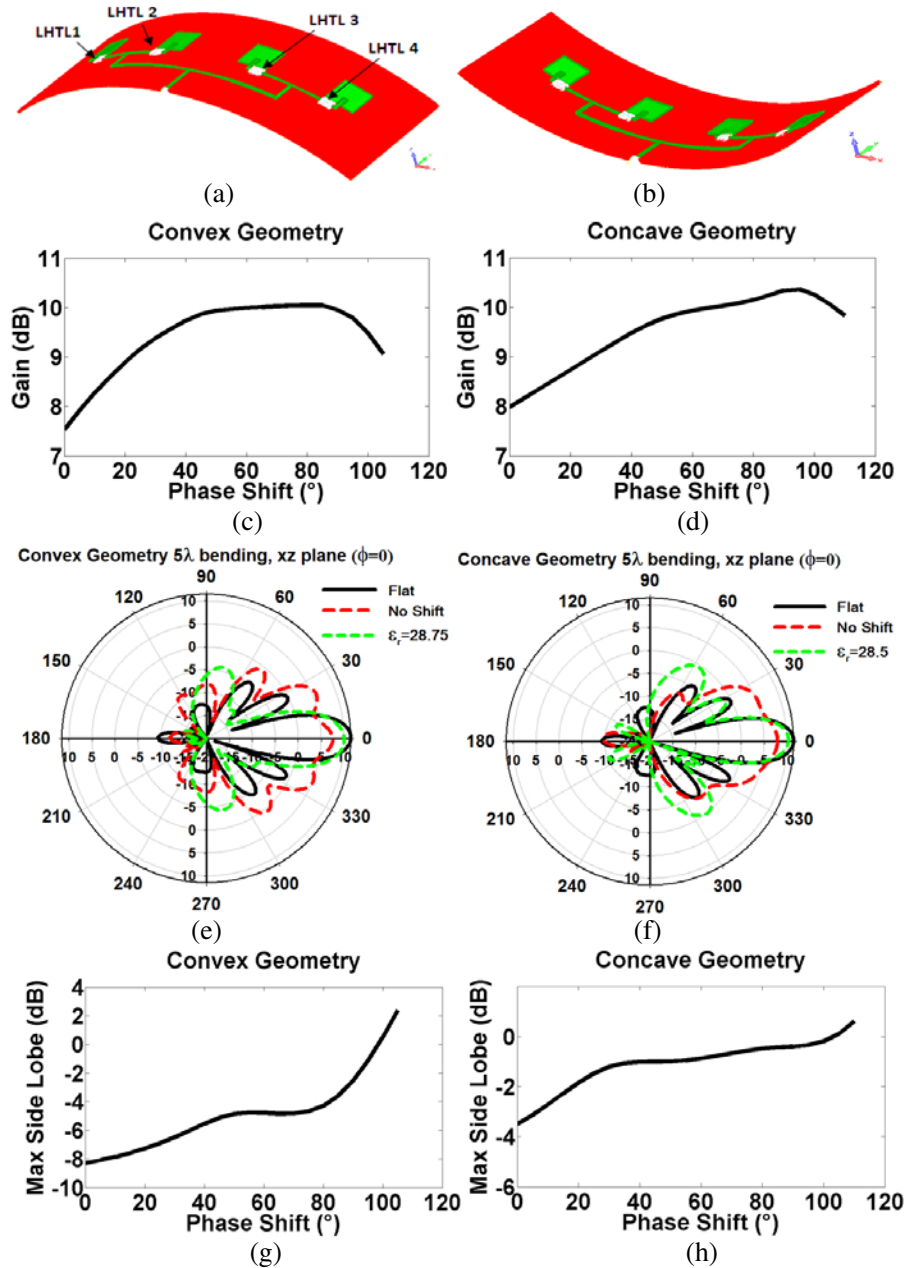
Figure 7. The conformal antenna array with (a) convex and (b) concave bending, the simulated gain in dB versus corresponding phase shift for the array with (c) convex and (d) concave geometry, the simulated E-plane radiation pattern for the array with (e) convex and (f) concave geometry, and the simulated maximum side lobe level for the array with (g) convex and (h) concave geometry.

as LHTL1 to LHTL4. Phase shifting can be achieved by adjusting the dielectric constant, ε_r, of BST/polymer material utilized in the phase shifters (see Fig. 1(b)). For the convex (concave) case the phase of both LHTL1 and LHTL4 (LHTL2 and LHTL3) was simultaneously shifted, whereas it was kept untuned for the other two. The maximum gain of the flat case and the bent cases with convex and concave geometries in untuned and tuned states with various values of ε_r are listed in Table 2. For the convex case, the corresponding phase shift in degrees with the achieved maximum gain is plotted in Fig. 7(c). The maximum gain was recovered when the phase shift was around 84°, which corresponds to $\varepsilon_r = 28.75$ (see Fig. 1(b)). This maximum compensation phase shift has only a 5.6% error compared to the calculated required phase shift obtained using (2). The 2D gain dependence on scan angle is plotted in Fig. 7(e) for the flat case, the convex case with no phase compensation, and the phase-compensated convex case with $\varepsilon_r = 28.75$. It can be seen that main lobe has been recovered when comparing the compensated and the uncompensated cases. But this has introduced a higher side lobe level as shown in Fig. 7(g), which reveals that a higher side lobe level is accompanied with a higher phase shift. A similar trend was observed for the concave geometry. The corresponding phase shift in degrees with the achieved maximum gain is plotted in Fig. 7(d). The maximum gain was recovered when the phase shift was around 95°, which corresponds to $\varepsilon_r = 28.5$ (see Fig. 1(b)). This maximum compensation phase shift has only a 6.7% error compared to the calculated required phase shift obtained using (2). The 2D gain dependence on scan angle is plotted in Fig. 7(f) for the flat case, the concave case with no phase compensation, and the phase-compensated concave case with $\varepsilon_r = 28.5$. The side lobe level of the compensated antenna has also increased for higher phase shift as shown in Fig. 7(h).

It is worth noting that a full recovery of radiation pattern is impossible with this method since it only attempts to compensate for the major effects caused by vertical displacement of elements, while neglecting other minor effects caused by factors such as horizontal displacement of elements or the change in the normal direct of surface currents.

Table 2. Comparison of the maximum gain for flat case and bent cases with convex and concave geometries for different dielectric constants.

Case	Flat	Geometry & Tuning	Bent & Untuned	Bent & Tuned					
		ε_r	30	29.75	29.5	29.25	28.75	28.5	28.25
Max Gain (dB)	11.48	Convex	7.53	8.47	9.39	9.94	10.05	9.62	9.27
	11.48	Concave	7.98	8.47	9.12	9.77	10.21	10.36	10.3

5. BEAM STEERING

The BST/polymer based LHTL phase shifters discussed in Section 2, specifically the microstrip design with radial stubs, can be employed to achieve beam steering. Fig. 8(a) shows the top view of a planar 1×4 antenna array with the radial stub phase shifters. The main beam can be redirected and controlled electronically by sequentially varying the relative phases of the RF signals propagating through the radial stub phase shifters. In practice, this can be achieved by adjusting the DC bias across the IDCs in the LHTL phase shifters, thus tuning the relative permittivity of the utilized ferroelectric material between the IDC fingers. To this end, a bias network needs to be designed and printed along with the phase shifters [16]. Here, we model this tuning behavior by changing the dielectric constant, ε_r, of the BST/polymer dielectric used in the phase shifters. Therefore, each phase shifter has a propagation constant different from the adjacent phase shifters. Sequentially decreasing or increasing ε_r of the utilized BST/polymer dielectrics from left to right in the phase shifters shown in Fig. 7(a), based on the range of values shown in Fig. 3(b), results in a negative or positive scan angle, respectively. Fig. 8(b) shows the 2D radiation patterns of the phased array antenna where the main beam is steered to both negative and positive scan angles. The 2D electric field maps in Fig. 8(c) show how the radiated fields from each element are delayed so that the main beam is directed to the desired direction.
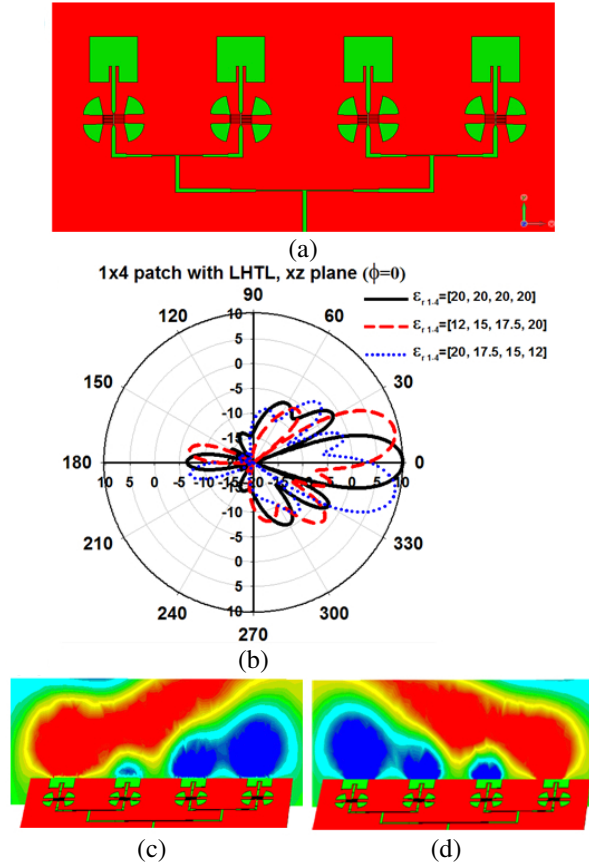
Figure 8. The 1×4 phased array using BST/polymer based LHTL phase shifter with radial stubs: (a) top view, (b) E-plane radiation pattern for various steered beam, and (c) E-field maps for steered beams.

6. CONCLUSION

In this work, a LHTL phase shifter design based on multiphase BST/polymer composites is proposed, which is compatible with processes used in printed electronics on flexible substrates. It is computationally assessed that the phase shifter can be utilized to compensate the gain loss of bent conformal arrays and to steer the beam of phased arrays. First, the impact of bending on antenna array performance is studied for convex and concave bending profiles. The full wave simulations show degradation in the antenna performance as bending is increased. The realized gain is enhanced by tuning the incorporated coplanar LHTL phase shifters. Second, a modified version of the LHTL phase shifter with radial stubs was used to beam steer the main beam of a planar phased array. The BST/polymer composite filled IDCs used in this work could be used in various RF applications where there is a demand for printable, compact, and versatile varactors.

ACKNOWLEDGMENT

REFERENCES

1. Seok, S. and J. Kim, "Design, fabrication, and characterization of a wideband 60 GHz bandpass filter based on a flexible PerMX polymer substrate," *IEEE Transactions on Components, Packaging*

and Manufacturing Technology, Vol. 3, No. 8, 1384–1389, 2013.

2. Byun, K., H. Subbaraman, X. Lin, X. Xu, and R. T. Chen, "A 3 μm channel, ink-jet printed CNTTFT for phased array antenna applications," *IEEE Texas Symposium on Wireless and Microwave Circuits and Systems (WMCS)*, 1–3, 2013.

3. Wang, C., J. Chien, K. Takei, T. Takahashi, J. Nah, A. M. Niknejad, and A. Javey, "Extremely bendable, high-performance integrated circuits using semiconducting carbon nanotube networks for digital, analog, and radio-frequency applications," *Nano Letters*, Vol. 12, No. 3, 1527–1533, 2012.

4. Zhang, K., J.-H. Seo, W. Zhou, and Z. Ma, "Fast flexible electronics using transferrable silicon nanomembranes," *Journal of Physics D: Applied Physics*, Vol. 45, No. 14, 143001, 2012.

5. Kim, S., B. Cook, T. Le, J. Cooper, H. Lee, V. Lakafosis, R. Vyas, R. Moro, M. Bozzi, A. Georgiadis, et al., "Inkjet-printed antennas, sensors and circuits on paper substrate," *IET Microwaves, Antennas & Propagation*, Vol. 7, No. 10, 858–868, 2013.

6. Waterhouse, R. B., *Printed Antennas for Wireless Communications*, Wiley Online Library, 2007.

7. Rida, A., L. Yang, R. Vyas, and M. M. Tentzeris, "Conductive inkjet-printed antennas on flexible low-cost paper-based substrates for RFID and WSN applications," *IEEE Antennas and Propagation Magazine*, Vol. 51, No. 3, 13–23, 2009.

8. Balanis, C. A., *Antenna Theory: Analysis and Design*, John Wiley & Sons Inc., New York, 2016.

9. Josefsson, L. and P. Persson, *Conformal Array Antenna Theory and Design*, Vol. 29, John Wiley & Sons Inc., New York, 2006.

10. Salonen, P., J. Kim, and Y. Rahmat-Samii, "Dual-band E-shaped patch wearable textile antenna," *IEEE Antennas and Propagation Society International Symposium*, Vol. 1, 466–469, 2005.

11. Schippers, H., G. Spalluto, and G. Vos, "Radiation analysis of conformal phased array antennas on distorted structures," *IET Conference Proceedings*, Vol. 3, 160–163, Jan. 2003.

12. Knott, P., "Deformation and vibration of conformal antenna arrays and compensation techniques," *Tech. Rep.*, FGAN-FHR Research Institute for High Frequency Physics and Radar Techniques Wachtberg, Germany, 2006.

13. Wincza, K. and S. Gruszczynski, "Influence of curvature radius on radiation patterns in multibeam conformal antennas," *IEEE 36th European Microwave Conference*, 1410–1413, 2006.

14. Seidel, T. J., W. S. T. Rowe, and K. Ghorbani, "Passive compensation of beam shift in a bending array," *Progress In Electromagnetics Research C*, Vol. 29, 41–53, 2012.

15. Braaten, B. D., S. Roy, S. Nariyal, M. Al Aziz, N. F. Chamberlain, I. Irfanullah, M. T. Reich, and D. Anagnostou, "A self-adapting flexible (SELFLEX) antenna array for changing conformal surface applications," *IEEE Transactions on Antennas and Propagation*, Vol. 61, No. 2, 655–665, 2013.

16. Sazegar, M., Y. Zheng, H. Maune, C. Damm, X. Zhou, J. Binder, and R. Jakoby, "Low-cost phased-array antenna using compact tunable phase shifters based on ferroelectric ceramics," *IEEE Transactions on Microwave Theory and Techniques*, Vol. 59, No. 5, 1265–1273, 2011.

17. Moussessian, A., L. Del Castillo, J. Huang, G. Sadowy, J. Hoffman, P. Smith, T. Hatake, C. Derksen, B. Lopez, and E. Caro, "Active membrane phased array radar," Jet Propulsion Laboratory, National Aeronautics and Space Administration, Pasadena, CA, 2005.

18. Chung, D. J., S. Bhattacharya, G. Ponchak, and J. Papapolymerou, "Recent advances in the development of a lightweight, flexible 16 × 16 antenna array with RF MEMS shifters at 14 GHz," *8th Annu. NASA Earth Sci. Technol. Conf.*, 2008.

19. Vaillancourt, J., H. Zhang, P. Vasinajindakaw, H. Xia, X. Lu, X. Han, D. C. Janzen, W.-S. Shih, C. S. Jones, M. Stroder, et al., "All ink-jet-printed carbon nanotube thin-film transistor on a polyimide substrate with an ultrahigh operating frequency of over 5 GHz," *Applied Physics Letters*, Vol. 93, No. 24, 243301, 2008.

20. Chen, M. Y., X. Lu, H. Subbaraman, and R. T. Chen, "Fully printed phased-array antenna for space communications," *SPIE Defense, Security, and Sensing, International Society for Optics and Photonics*, 731–814, 2009.

21. Chen, M. Y., D. Pham, H. Subbaraman, X. Lu, and R. T. Chen, "Conformal ink-jet printed-band phased-array antenna incorporating carbon nanotube field-effect transistor based reconfigurable true-time delay lines," *IEEE Transactions on Microwave Theory and Techniques*, Vol. 60, No. 1, 179–184, 2012.

22. Subbaraman, H., D. T. Pham, X. Xu, M. Y. Chen, A. Hosseini, X. Lu, and R. T. Chen, "Inkjetprinted two-dimensional phased-array antenna on a flexible substrate," *IEEE Antennas and Wireless Propagation Letters*, Vol. 12, 170–173, 2013.

23. Pham, D. T., H. Subbaraman, M. Y. Chen, X. Xu, and R. T. Chen, "Light weight and conformal 2-bit, 1×4 phased-array antenna with CNT-TFT-based phase shifter on a flexible substrate," *IEEE Transactions on Antennas and Propagation*, Vol. 59, No. 12, 4553–4558, 2011.

24. Gevorgian, S., *Ferroelectrics in Microwave Devices, Circuits and Systems: Physics, Modeling, Fabrication and Measurements*, Springer Science & Business Media, 2009.

25. Liou, J. W. and B. S. Chiou, "Dielectric tunability of barium strontium titanate/silicone-rubber composite," *Journal of Physics: Condensed Matter*, Vol. 10, No. 12, 2773, 1998.

26. Hadik, N., A. Outzourhit, A. Elmansouri, A. Abouelaoualim, A. Oueriagli, and E. Ameziane, "Dielectric behavior of ceramic (BST)/epoxy thick films," *Active and Passive Electronic Components*, 2009.

27. Wang, H., F. Xiang, and K. Li, "Ceramic-polymer $Ba_{0.3}Sr_{0.7}TiO_3$/Poly(Methyl Methacrylate) composites with different type composite structures for electronic technology," *International Journal of Applied Ceramic Technology*, Vol. 7, No. 4, 435–443, 2010.

28. Hu, T., J. Juuti, and H. Jantunen, "RF properties of BST-PPS composites," *Journal of the European Ceramic Society*, Vol. 27, No. 8, 2923–2926, 2007.

29. Hu, T., J. Juuti, H. Jantunen, and T. Vilkman, "Dielectric properties of BST/polymer composite," *Journal of the European Ceramic Society*, Vol. 27, No. 13, 3997–4001, 2007.

30. Haghzadeh, M., L. M. Bhowmik, C. Armiento, and A. Akyurtlu, "Printed tunable miniaturized frequency selective surface with BST/polymer composite filled interdigital capacitors," *IEEE USNCURSI Radio Science Meeting (Joint with AP-S Symposium)*, 154–154, 2014.

31. Haghzadeh, M. and A. Akyurtlu, "RF measurement technique for characterizing printed ferroelectric dielectrics," *37th Annual Meeting & Symposium, Antenna Measurement Techniques Association (AMTA)*, 2015.

32. Haghzadeh, M., C. Armiento, and A. Akyurtlu, "Electrostatic and full wave simulations of interdigitated BST varactors with buried plates," *IEEE 31st International Review of Progress in Applied Computational Electromagnetics (ACES)*, 1–2, 2015.

33. Lai, A., T. Itoh, and C. Caloz, "Composite right/left-handed transmission line metamaterials," *IEEE Microwave Magazine*, Vol. 5, No. 3, 34–50, 2004.

34. Erker, E. G., A. S. Nagra, Y. Liu, P. Periaswamy, T. R. Taylor, J. Speck, R. York, et al., "Monolithic Ka-band phase shifter using voltage tunable $BaSrTiO_3$ parallel plate capacitors," *IEEE Microwave and Guided Wave Letters*, Vol. 10, No. 1, 10–12, 2000.

35. Vélu, G., K. Blary, L. Burgnies, J. C. Carru, E. Delos, A. Marteau, and D. Lippens, "A $310°/3.6$-dB K-band phaseshifter using paraelectric BST thin films," *IEEE Microwave and Wireless Components Letters*, Vol. 16, No. 2, 87–89, 2006.

36. Sherman, V. O., T. Yamada, A. Noeth, N. Setter, M. Mandeljc, B. Malic, M. Kosec, and M. Vukadinovic, "Microwave phase shifters based on sol-gel derived $Ba_{0.3}Sr_{0.7}TiO_3$ ferroelectric thin films," *IEEE EuMIC European Microwave Integrated Circuit Conference*, 497–500, 2007.

37. Satish, G. N., K. Srivastava, A. Biswas, and D. Kettle, "A via-free left-handed transmission line with radial stubs," *IEEE APMC Asia Pacific Microwave Conference*, 2501–2504, 2009.

38. Bhowmik, L. M., C. Armiento, A. Akyurtlu, W. Miniscalco, J. Chirravuri, and C. McCarroll, "Design and analysis of conformal Ku-band microstrip patch antenna arrays," *2013 IEEE International Symposium on Phased Array Systems & Technology*, 815–820, 2013.

39. Haupt, R. L., *Antenna Arrays: A Computational Approach*, John Wiley & Sons Inc., New York, 2010.